Adhesion Plaque Formation Dynamics between Polymer Vesicles in the Limit of Highly Concentrated Binding Sites

Jin Nam and Maria M. Santore*

Department of Polymer Science and Engineering, University of Massachusetts−Amherst, 120 Governors Drive, Amherst, Massachusetts 01003

Received February 23, 2007. In Final Form: April 7, 2007

This work examines the process of adhesion plaque formation between pairs of copolymer vesicles presenting dense surface concentrations of avidin (NeutrAvidin) and biotin. Micropipet aspiration maintains constant membrane tension, as the low-tension vesicle membrane spreads over a second, more tensed vesicle. Spreading rates near 1 μm/s but as high as 7 μm/s (the adhesion plaque diameter) and contact angle growth rates of 2−14 deg/s are observed. The ultimate contact angles, in the range of 120−140°, are independent of membrane tension and also exceed those previously reported. Adhesion plaque formation occurs in three phases: an initial step in which contact is established, typically lasting from a few seconds to a minute, an abrupt jump into contact in which both vesicles undergo substantial deformation, and a slower continued growth of the contact angle and area. Vesicle pairs are irreversibly bound at the plaque such that attempts to peel them apart cause membrane rupture at critical tensions as high as 4 mN/m, setting a lower bound on the interfacial strength. When the quantity $\tau(1 - \cos\theta)$ (with τ the membrane tension and θ the contact angle) is plotted as a function of time during plaque formation for different values of τ, the curves fail to collapse, indicating the chemical driving force for adhesion greatly exceeds the mechanical resisting tension.

Introduction

Developing an understanding of membrane adhesion and a means to control it in biomimetic systems is important for a number of reasons: At the fundamental level, well-defined model membranes can provide quantitative predictive insight into key aspects of cellular behavior, including cell adhesion, signaling, and other functions relying on cell membrane tension. Membrane adhesion fundamentals also must form the basis for design rules for applications such as targeted delivery systems (liposomes and polymeric vesicles), artificial white blood cells, and membrane-based microscavengers for environmental cleanup.

Our understanding of membrane adhesion at the supermolecular or micrometer scale has evolved substantially in the past several decades, especially with the advent of sensitive force-based methods (for instance, AFM, colloidal probe, and micropipet aspiration). Most textbooks on the subject of membrane adhesion address its physical chemical (van der Waals, electrostatic, donor−acceptor) and mechanical physical origins (bending fluctuations), while much of the recent theory also focuses on equilibrium aspects of adhesion such as vesicle shape.[1,2] As many model adhesive membranes employ avidin/biotin molecules,[3−8] additional considerations must take into account the incorporation of strongly binding ligand−receptor pairs, including the discrete nature of the stickers[9] along with nonequilibrium and kinetic aspects of adhesion, for instance, energy dissipation and spreading dynamics.

One of the most important ways to characterize an interface is through the adhesion strength, often determined by studies in which the interface is separated, for instance by peeling. Applied to weakly binding membrane systems, as with a dual-pipet technique, the contact angle allows determination of the reversible work of adhesion through a modified Young equation.[10] For more strongly adherent situations, peeling studies access interfacial strength;[11] however, the values reported exceed the reversible work of adhesion by the effort expended to deform the membrane[12] and are likely dependent on the rate of the applied peeling force.[13] When adhesion is completely irreversible (meaning that the strength of the contact area is greater than that of the membranes themselves), then the membrane lysis tension sets the lower bound for the adhesion strength. (That is, the actual adhesion strength cannot be quantified experimentally.) Relevant to the current work, the lysis tensions of most giant unilamellar copolymer membranes exceed those of liposomes, increasing the range of adhesion strengths that can be measured experimentally.[14] However, in the case of avidin−biotin binding, one still expects multiple ligand−receptor interactions within an adhesive plaque to exceed the lysis strength of copolymer membranes.

Separate from the issue of adhesion strength is the process by which adhesive bonds form at the molecular level and by which macroscopic adhesive contact grows. With strongly or irreversibly binding membrane systems, especially where discrete binding sites produce adhesion, one envisions certain physical or mechanical processes contributing to the adhesion mechanism and rate:[15,16] upon close approach of two membrane surfaces,

(1) Capovilla, R.; Guven, J. *Phys. Rev. E* **2002**, *66*.
(2) Tordeux, C.; Fournier, J. B.; Galatola, P. *Phys. Rev. E* **2002**, *65*.
(3) Helm, C. A.; Knoll, W.; Israelachvili, J. N. *Proc. Natl. Acad. Sci. U.S.A.* **1991**, *88*, 8169−8173.
(4) Pignataro, B.; Steinem, C.; Galla, H. J.; Fuchs, H.; Janshoff, A. *Biophys. J.* **2000**, *78*, 487−498.
(5) Jeppesen, C.; Wong, J. Y.; Kuhl, T. L.; Israelachvili, J. N.; Mullah, N.; Zalipsky, S.; Marques, C. M. *Science* **2001**, *293*, 465−468.
(6) NopplSimson, D. A.; Needham, D. *Biophys. J.* **1996**, *70*, 1391−1401.
(7) Kim, D. H.; Klibanov, A. L.; Needham, D. *Langmuir* **2000**, *16*, 2808−2817.
(8) Cuvelier, D.; Nassoy, P. *Phys. Rev. Lett.* **2004**, *93*.
(9) Zuckerman, D. M.; Bruinsma, R. F. *Phys. Rev. E* **1998**, *57*, 964−977.
(10) Evans, E.; Needham, D. *Macromolecules* **1988**, *21*, 1822−1831.
(11) Lin, J. J.; Silas, J. A.; Bermudez, H.; Milam, V. T.; Bates, F. S.; Hammer, D. A. *Langmuir* **2004**, *20*, 5493−5500.
(12) Chaudhury, M. K. *J. Phys. Chem. B* **1999**, *103*, 6562−6566.
(13) Ghatak, A.; Vorvolakos, K.; She, H. Q.; Malotky, D. L.; Chaudhury, M. K. *J. Phys. Chem. B* **2000**, *104*, 4018−4030.
(14) Bermudez, H.; Brannan, A. K.; Hammer, D. A.; Bates, F. S.; Discher, D. E. *Macromolecules* **2002**, *35*, 8203−8208.
(15) de Gennes, P. G.; Puech, P. H.; Brochard-Wyart, F. *Langmuir* **2003**, *19*, 7112−7119.

10.1021/la700542t CCC: $37.00
Published on Web 05/25/2007

complementary species on opposing sides of a fluid-filled gap must register via diffusion in-plane within each membrane and via local reorientations which include the chemical groups that anchor them to each side of the interface. Once the binding sites reach sufficient proximity and orientation, binding occurs. For many such binding events to produce an adhesion plaque (as opposed to just a few bonds), the membrane itself must deform to produce a growing contact area, hence the spreading process.[17−20] Separate from spreading, additional bonds may form across the gap to strengthen an established adhesion plaque. Thus, establishing adhesive contact involves translational[16] and configurational[5] diffusive processes and membrane deformation, in addition to the binding kinetics of complementary groups across a gap. In addition to these molecular processes, membrane bending in flaccid systems gives rise to repulsions (through fluctuations)[21] and the development of adhesion through the initiation of adhesive islands.[22]

The current work examines adhesive plaque formation dynamics of unilamellar copolymer membranes, driven by avidin−biotin binding. Here, a dual-pipet method maintains relatively high membrane tensions (on the order of 0.1 or 1 mN/m) relative to studies in which flaccid vesicles settle on rigid surfaces and develop patchwise adhesion. The current work advances previously published results[6,8,11,17,19,23] in that here (1) membrane tension is controlled, (2) irreversible membrane−membrane contact is studied, and (3) the limit of very dense binding sites is studied. The latter constraint reduces the potential contribution of translational diffusion to the plaque formation kinetics, since the biotins on one interface need not diffuse (in plane) far to align with an avidin on the opposing membrane. Hence, adhesion and spreading kinetics will be dominated by configurational motions of the ligands and receptors, membrane deformation processes, and the underling ligand−receptor binding kinetics. The findings include relatively fast and sudden growth of the contact area and angle compared with that described in the literature. It turns out that the interfaces could not be peeled apart; however, in this paper we present a discussion of adhesion strength in the context of driving forces for and resisting forces against spreading of the contact zone. The limit of membrane cohesion strength, which sets a lower bound for the interfacial strength of the adhesion plaque, exceeds values in other reports.

Experimental Description

Materials. Vesicles were made from the commercial copolymer surfactant Dow Corning 5329, obtained from Dow Corning. Dow Corning product literature reports DC 5329 to be vesicle-forming, with its chemical structure containing polyethylene glycol arms averaging 12 monomers in length on a poly(dimethylsiloxane) (PDMS) polymer. We estimate DC5329 to be roughly of 3000 molecular weight, with one 12-unit oligomeric PEG arm for each 1500 molecular weight unit of polymer, on the basis of manufacturer's reports and the literature: Comb-type copolymers of PEG-12 on PDMS, despite their polydispersity in the EO length and distribution of PEG arms on the PDMS backbone, are known to form giant multilamellar vesicles, when there is one PEG-12 for every 1450 molecular weight unit of polymer.[24,25] Indeed this proportion of EO to hydrophobic backbone (30 wt % EO, 70 wt % hydrophobe) is similar to that reported for nonionic vesicle-forming diblock copolymers with different hydrophobic chemistry.[14,26,27] The molecular weight of 3000 was estimated from the bulk melt viscosity of DC5329, reported from its product literature, along with viscosity and molecular weight values of similar compounds of known molecular weight from other companies, for instance, Gelest.[28]

Classical electroformation methods on platinum wires[29] were successful in producing large numbers of giant unilamellar vesicles of DC5329, appropriate for quantitative micropipet studies. Electroforming was done in sucrose solutions near 250 mOsm. Adhesion studies and other vesicle manipulations were conducted in phosphate-buffered (pH 7.4) glucose solutions having a total osmolarity near 270 mOsm.

Biotinylated vesicles were made by chemical modification of the DC5329 prior to vesicle electroformation, following an established tosylation protocol.[30,31] Here, any possible residual solvents were removed from the DC5329 by drying under vacuum overnight, resulting in 0.5 wt % loss. The DC5329 was then dissolved in DMF (dimethylformamide; Aldrich), and excess toluenesulfonyl chloride (Aldrich) was added, along with the equilivalent molar amount of DMAP (4-(dimethylamino)pyridine). The mixture was stirred at 60 °C for 2 h and then the DMF removed under vacuum. Pentane, a nonsolvent for unreacted tosyl chloride and DMAP, was then used to removed these species by precipitation. The tosylated 5329 was recovered as a filtration supernatant and then reacted with excess 5-biotinamidopentylamine (Pierce Biotechnology Inc., Rockford, IL) in DMF at 60 °C for 24 h. Excess biotin was tolerated during the electoforming process and simply washed away in the subsequent vesicle handling such that only the conjugated biotin species, b-5329, contributed to adhesion.

Fluorescein-tagged NeutrAvidin was purchased from Pierce Biotechnology Inc., chosen because of its reported lower nonspecific interactions compared with those of avidin[32,33] and its economy compared with that of streptavidin. F-NeutrAvidin-coated vesicles were made by incubating biotinylated vesicles in phosphate-buffered glucose solutions of F-NeutrAvidin (0.05 mg/mL) and then recovering the vesicles by centrifugation (or settling under gravity).

Methods. A micropipet aspiration apparatus, following previously published designs,[11,34,35] employed Narishige micromanipulators mounted on a Nikon Eclipse TE300 optical/fluorescence microscope, with primary use of a 40× Hoffman contrast objective, in addition to several others. Suction to the micropipets was controlled with siphon manometers and measured with Validyne (Northridge, CA) transducers. The micropipets themselves were drawn on a Kopf model 730 micropipet puller (Tujunga, CA) and finished on a Technical Products International (St. Louis, MO) microforge to give

(16) Brochard-Wyart, F.; de Gennes, P. G. *Proc. Natl. Acad. Sci. U.S.A.* **2002**, *99*, 7854−7859.
(17) Boulbitch, A.; Guttenberg, Z.; Sackmann, E. *Biophys. J.* **2001**, *81*, 2743−2751.
(18) Guttenberg, Z.; Lorz, B.; Sackmann, E.; Boulbitch, A. *Europhys. Lett.* **2001**, *54*, 826−832.
(19) Kloboucek, A.; Behrisch, A.; Faix, J.; Sackmann, E. *Biophys. J.* **1999**, *77*, 2311−2328.
(20) Bernard, A. L.; Guedeau-Boudeville, M. A.; Jullien, L.; di Meglio, J. M. *Langmuir* **2000**, *16*, 6809−6820.
(21) Israelachvili, J. N.; Wennerstrom, H. *J. Phys. Chem.* **1992**, *96*, 520−531.
(22) Albersdorfer, A.; Feder, T.; Sackmann, E. *Biophys. J.* **1997**, *73*, 245−257.
(23) Lin, J. J.; Bates, F. S.; Hammer, D. A.; Silas, J. A. *Phys. Rev. Lett.* **2005**, *95*.
(24) Hill, R. M.; He, M. T.; Lin, Z.; Davis, H. T.; Scriven, L. E. *Langmuir* **1993**, *9*, 2789−2798.
(25) Lin, Z.; Hill, R. M.; Davis, H. T.; Scriven, L. E.; Talmon, Y. *Langmuir* **1994**, *10*, 1008−1011.
(26) Bermudez, H.; Hammer, D. A.; Discher, D. E. *Langmuir* **2004**, *20*, 540−543.
(27) Discher, B. M.; Won, Y. Y.; Ege, D. S.; Lee, J. C. M.; Bates, F. S.; Discher, D. E.; Hammer, D. A. *Science* **1999**, *284*, 1143−1146.
(28) With comb-type polymers, melts were likely unentangled, with viscosity proportional to the molecular weight, allowing us to estimate the DC5329 molecular weight.
(29) Dimitrov, D. S.; Angelova, M. I. *Bioelectrochem. Bioenerg.* **1988**, *19*, 323−336.
(30) Nilsson, K.; Norrlow, O.; Mosbach, K. *Acta Chem. Scand., Ser. B: Org. Chem. Biochem.* **1981**, *35*, 19−27.
(31) Nilsson, K.; Mosbach, K. *Eur. J. Biochem.* **1980**, *112*, 397−402.
(32) Vanroy, N.; Mangelschots, K.; Speleman, F. *Trends Genet.* **1993**, *9*, 71−72.
(33) Hiller, Y.; Gershoni, J. M.; Bayer, E. A.; Wilchek, M. *Biochem. J.* **1987**, *248*, 167−171.
(34) Longo, M. L.; Waring, A. J.; Hammer, D. A. *Biophys. J.* **1997**, *73*, 1430−1439.
(35) Santore, M. M.; Discher, D. E.; Won, Y. Y.; Bates, F. S.; Hammer, D. A. *Langmuir* **2002**, *18*, 7299−7308.

straight tips with inner diameters in the range of 5−10 μm. Membrane mechanics and adhesion studies were carried out in home-built glass-walled aspiration chambers,[11] into which one or two micropipets were inserted. These chambers were filled with phosphate-buffered glucose, and then a small amount of sucrose-based vesicle suspension (10−20 uL) was added. The resulting situation, in which the vesicle interiors were filled with sucrose solution while the exterior was phosphate-buffered glucose, was useful for several reasons: First, with the low membrane permeability to water and sugar, an osmotic membrane tension was maintained throughout experiments, keeping the vesicle volume essentially constant on the time scales of study. The refractive index difference between the interior sucrose and exterior glucose solutions facilitated imaging of the vesicles in phase contrast and Hoffman imaging. Finally, the density difference between the interior and exterior sugar solutions caused the vesicles to settle under gravity or centrifugation, aiding in their manipulation.

In studies of membrane mechanics, each vesicle was aspirated into a micropipet, and the suction was first increased relatively quickly to draw out any wrinkles and tethers in the membrane. The suction was then decreased to nearly zero to initiate the experiment: The suction was then increased again, this time stepwise and relatively slowly (0.1 mN/m/s between pulling steps, holding the tension for several seconds for each datum before slowly increasing it again) to obtain approximately 10 data points at increasing membrane tensions. This process continued until the vesicle broke. Vesicle images, recorded on video, were analyzed to obtain the membrane area at each suction level, and the LaPlace equation was applied to translate the suction values to the isotropic membrane tension, τ:

$$\tau = P_s R_p/(2 - 2R_p/R_v) \quad (1)$$

Here P_s is the suction pressure, R_p the pipet radius, and R_v the radius of the spherical part of the vesicle outside the pipet. The plot of membrane tension as a function of areal strain gives the area expansion modulus, K_a, as the slope. The lysis conditions are also apparent. While some of the data for greatly functionalized membranes will display a substantial upward curvature for stress as a function of strain, we believe this to be a true strain hardening rather than the influence of bending on the measurement of K_a. The K_a determinations were done in regions where membrane bending fluctuations were suppressed by membrane tension. Therefore, throughout this paper, we use K_a rather than apparent K_a.

The membrane adhesion studies reported here were essentially spreading experiments, in which an attempt was made to parallel previously published strategies.[6,10] One vesicle, held at low tension, was allowed to spread over a second vesicle, held at higher tension. In such a situation, the high-tension vesicle usually maintains a spherical bulb outside the pipet, allowing for consistent geometrical design of the contact region and interpretation of the results in terms of a contact angle−Young equation analysis or peeling work. While copolymer vesicles are typically more robust than liposomes in their lysis stresses and strains, this work reports weakening of the membrane by dense functionalization, especially for the avidin-coated vesicles. Therefore, the Neutravidin-coated vesicle (of the avidin−biotin pair) was set to the low tension, while the biotinylated vesicle was maintained at the higher of the two tensions.

Execution of the adhesion protocol involved insertion of two pipets into a chamber filled with buffered glucose solution, which contained biotinylated vesicles (in one region of the chamber) and biotin vesicles that had been conjugated with F-NeutrAvidin (in another region of the chamber). The two could be distinguished due to the fluorescence of the latter. A biotinylated vesicle was aspirated into one micropipet, while a NeutrAvidin-conjugated vesicle was aspirated into the second pipet. The vesicles were then subjected to a K_a measurement to ensure that each was unilamellar. (A multilamellar vesicle will have a substantially larger K_a value than a unilamellar vesicle.) The biotinylated vesicle was then held at a relatively high suction, while the avidin vesicle was held at lower suction. The two vesicles were brought into contact, and the progress of their adhesion and spreading at constant tension and fixed pipet separation was recorded on video. Often, the adhesion run terminated in the escape of one of the two vesicles from its pipet. Subsequently, attempts were made to reaspirate the vesicle and to pull the pair apart, a separate peeling study.

Results and Discussion

Receptor Surface Density. The average spacing between biotins on biotinylated vesicles is estimated from basic arguments: To the extent that the biotinylation chemistry successfully labeled all terminal hydroxyls on the PEG side arms, and estimating a nonbiotinylated membrane mass of 5 mg/m^2 (from a hydrophobic membrane core thickness of about 5 nm[24]), the nominal 12-EO-arm graft density of 1/1500 molecular weight unit of polymer leads to a biotinylation surface concentration of 1.5 per nm^2, an extremely dense arrangement of ligands. This figure represents an upper limit on the biotin surface density of the "100%" biotinylated vesicles.

The relative densities of avidin receptors on F-NeutrAvidin-saturated vesicles were assessed from the analysis of fluorescence images of the F-NeutrAvidin-conjugated b-vesicles in Figure 1. Here, the biotinylation density was varied by mixing b-5329 and native 5329 in different proportions prior to electroformation. The resulting vesicles, with their different biotinyl surface densities, were then incubated in a solution of F-NeutrAvidin, sufficient to saturate the biotinyl surface groups, and recovered by centrifugation. A series of F-NeutrAvidin-coated vesicles, with underlying biotinylated fractions ranging from 0% to 100% are presented in Figure 1A,B (which shows the vesicle images and the typical edge-bright cross-sectional profiles) and quantified in Figure 1C. In Figure 1C, the fluorescence from F-NeutrAvidin is linear in biotinyl functionality at low concentrations up to about 50% nominal biotinylation functionality. At greater biotin surface densities, the fluorescence from the bound F-NeutrAvidin does not further increase, suggesting no further binding of F-NeutrAvidin.

The fluorescence data in Figure 1C follow expectations: in the dilute limit, all exterior surface biotins bind F-NeutrAvidin conjugates, giving linearity between the biotin (and F-NeutrAvidin) surface density and the fluorescence signal. At saturation, however, F-NeutrAvidin binding becomes limited by the vesicle capacity. If 100% biotin corresponds to a receptor density of 1.5 per nm^2, the avidin saturation at 50% biotin corresponds to 0.75 avidin/nm^2, or 1.3 nm^2/F-NeutrAvidin (if each avidin binds one biotin). The F-NeutrAvidin spacing at saturation (50−100% biotin vesicle makeup) may be as much as 4 times greater (5.2 nm^2/avidin) since avidins have four biotin binding sites. The estimated F-NeutrAvidin saturation level is therefore consistent with the avidin size (4.1 × 5.5 × 1.5 nm),[6] although if all the avidin pockets were occupied with biotin, the vesicles would be nonadhesive.

The current adhesion study focuses on the limit of highly concentrated receptor density. Therefore, fully biotinylated vesicles were paired with F-NeutrAvidin-saturated versions of the same. From the calculations and fluorescence data, it is estimated that biotinylated vesicle surfaces with an approximate density of 1.5 biotins/nm^2 were paired with vesicles presenting approximately 0.19−0.75 avidin/nm^2, the upper limit for each species.

Membrane Mechanics. Given the large ligand and receptor densities on the vesicles in this study, we considered the possibility that membrane functionalization might alter the membrane mechanics. Figure 2 compares the stretching behavior of native DC5329 and fully biotinylated vesicles with F-NeutrAvidin-saturated vesicles. The data are typical of the 10 vesicles tested at each level of functionality. The unfunctionalized membrane follows a linear stress−strain relationship with an average lysis

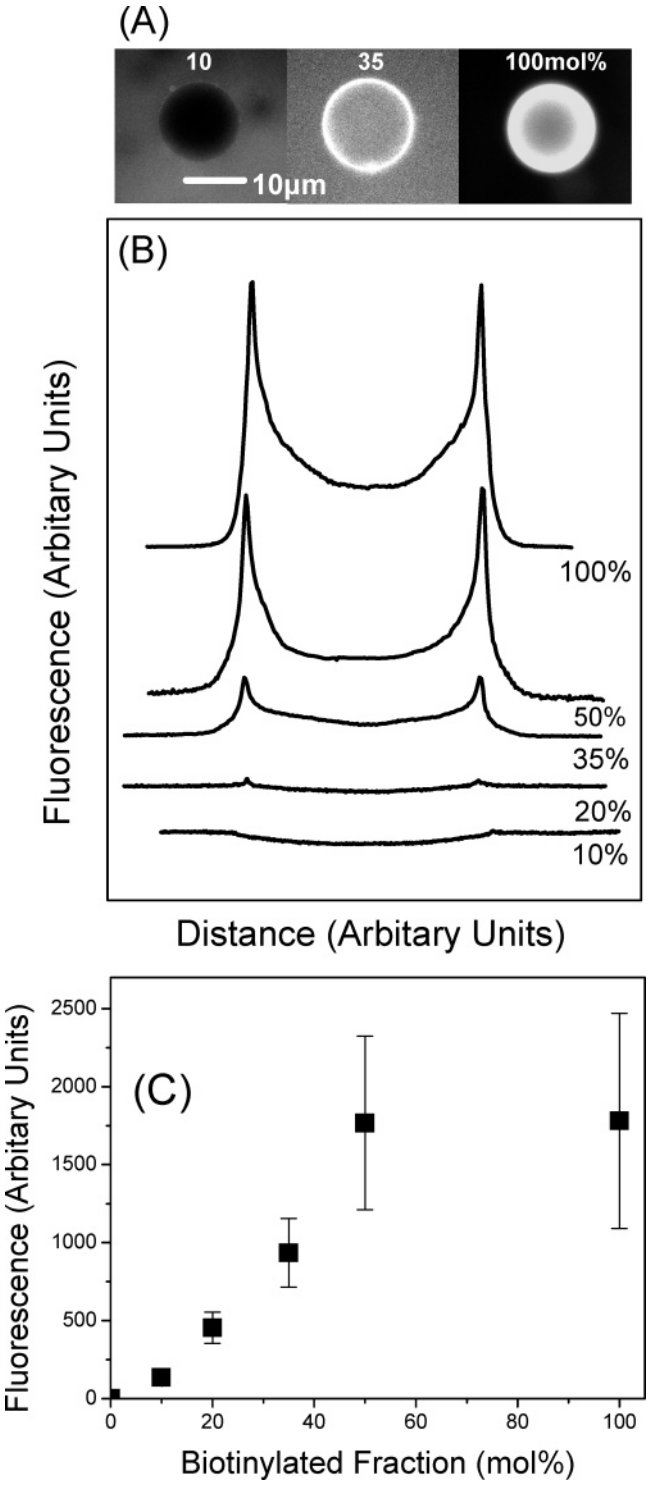

Figure 1. (A) Fluorescent micrographs of biotinyl-DC5329 vesicles with 10%, 35%, and 100% biotinyl modification and surface saturation by F-NeutrAvidin. (B) Line profiles corresponding to vesicles of different labeling densities. (C) Fluorescence as a function of biotinyl functionality.

strain near 8% and a K_a of 92 mN/m, slightly less than values reported for PBD−PEO and PEE−PEO membranes.[27] The fully biotinylated membrane is more easily stretched, with a lower K_a value and a greater lysis strain but a lower lysis tension. Conjugation with a saturated layer of F-NeutrAvidin increases the stretching modulus somewhat, relative to that of the biotinylated vesicles, but further compromises the membrane integrity, giving more fragile lysis conditions. These observations suggest that some of the functional groups may, to some extent,

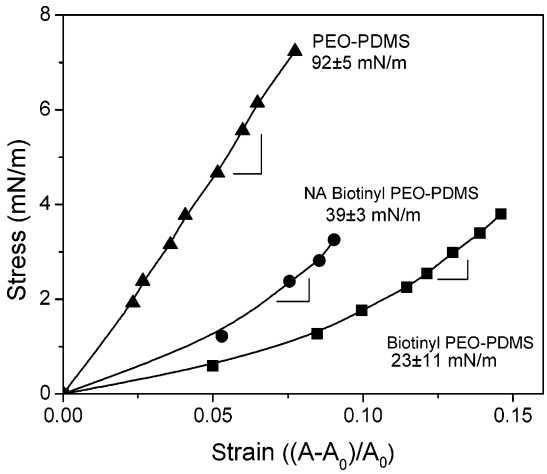

Figure 2. Typical stress−strain plots comparing vesicles of DC5329, 100% b-DC5329, and NeutrAvidin-saturated 100% b-DC5329. The modified membrane strain stiffens, and the regions where we assessed the slope (Ka) are indicated. Tolerances on Ka represent variations from about 10 vesicles of each type.

be buried beneath the outer corona of the vesicle, an important consideration for adhesion studies.

The greater impact of functionalization on mechanical properties in this study compared with others in the literature[11,36] may be a result of the large number of functionalizable groups on the DC5329, facilitated by the graft architecture. With 12 PEG units (hydroxyl-terminated) for roughly every 1500 molecular weight unit of polymer, full functionalization means 2 or more times the biotin density compared with systems of higher molecular weight and chain end functionality.

The lysis conditions in Figure 2 place limits on the conditions that can be applied during the micropipet-based adhesion studies. Because the biotinylated vesicles were more robust than those having F-NeutrAvidin conjugation, the biotinylated vesicles were chosen for the higher tension component of each vesicle pair, held at tensions below 2 mN/m (well below the 4 mN/m lysis tension to avoid statistical breakage). The more fragile F-NeutrAvidin-conjugated vesicles were held at lower tension and allowed to spread over the biotinylated vesicles.

Adhesion Studies. *Spreading at Constant Tension*. Figure 3 shows images from an adhesion experiment in which both vesicles are held at constant tension: the left biotinylated vesicle at 1.45 mN/m and the right avidin-coated vesicle at 0.55 mN/m. The projections of the two vesicles inside the pipets are indicated by arrows. In this run, the first 62 s following initial contact shows barely discernable increases in the contact area and angle. Then, beyond 62 s, adhesion and spreading advance suddenly, along with rapid and dramatic increases in both contact area and angle. Adhesion is sufficiently strong that, in addition to one vesicle spreading over the second, both vesicles deform, manifested by a decrease in vesicle dimension in the direction perpendicular to the pipets. At times longer than this rapid contact (beyond 69 s), adhesion continues to evolve further, as evidenced by slower changes in the contact angle and projection lengths. Ultimately, the right (low tension) vesicle continues to spread over the higher tension vesicle on the left, until the right vesicle escapes its pipet.

The example in Figure 3 typifies the constant-tension runs in our study, involving 18 vesicles, with the high-tension biotin side held from 0.1 to 2.5 mN/m and the lower tension avidin side

(36) Lin, J. J.; Ghoroghchian, P.; Zhang, Y.; Hammer, D. A. *Langmuir* **2006**, *22*, 3975−3979.

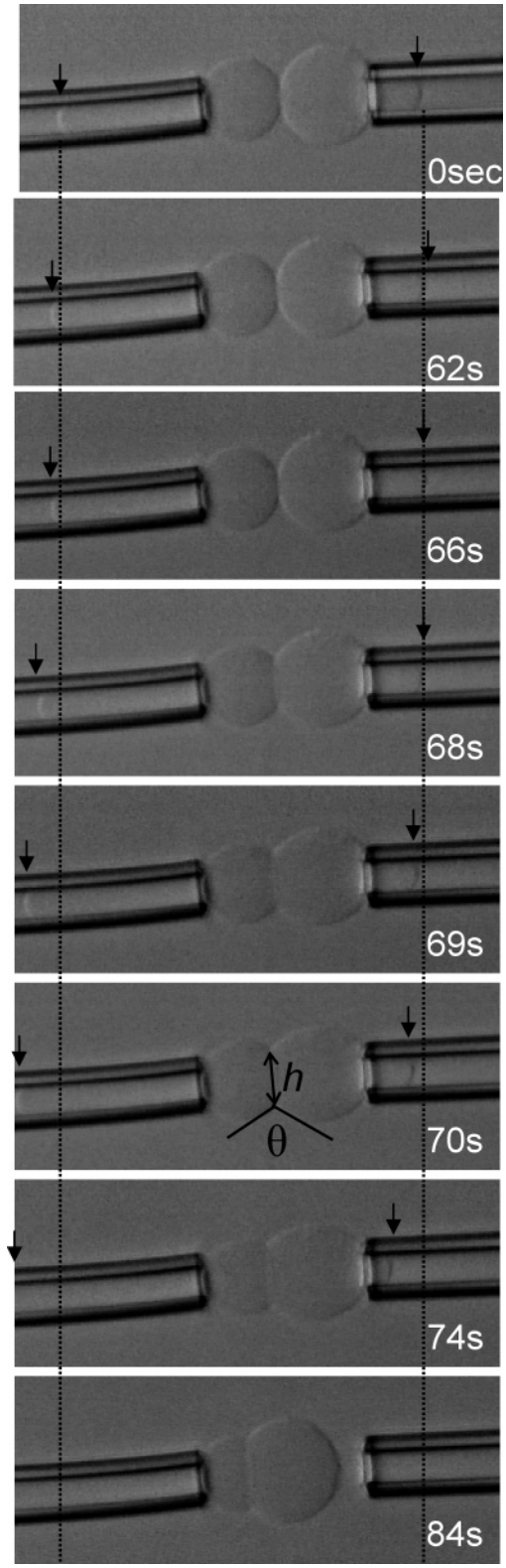

Figure 3. A series of video images illustrating typical vesicle adhesion dynamics at constant suction. The left (b-DC5329) vesicle is held at high tension, while that on the right is at lower tension. Dashed lines indicate the initial projections in the two pipets. The left projection becomes progressively longer and eventually leaves the video frame. θ and h are defined here.

held at 0.05−1.3 mN/m. The ratio of high tension to low tension varied from 1.5 to 10. In describing these results, we identified three general phases of the spreading process: Phase 1, prespreading, begins with the initial macroscopic contact and persists up to the period of rapid growth. It involves very minor but real changes in vesicle shape, as intimate contact is established. For the 18 vesicles examined, phase 1 lasted no longer than 90 s, and for 15 of these vesicles, it lasted less than 20 s. In many cases, that is, for 11 vesicles, phase 1 was quite short, lasting 5 s or less. Indeed, while Figure 3 exhibits a long phase 1 prespreading phase, the subsequent adhesive behavior was average relative to that of other vesicles in the study. The time variations of phase 1 may result from variations in the cleanliness of the vesicle surface at the nanometer scale. Even a few nanoscale particulates near the point of initial contact will impede the close membrane approach needed for avidin−biotin engagement across the gap. Of note, we observed no significant correlation between the imposed membrane tension and the duration of phase 1.

Unlike the prespreading phase 1, which is typified by subtle changes, phase 2, rapid adhesion, is marked by rapid and dramatic alterations in vesicle shape. In a matter of seconds, the contact zone grows, the contact angle increases, the main parts of the vesicles abandon their spherical shapes to become somewhat flattened or ellipsoidal, and the projection lengths in the pipets evolve. Watching the video tape, phase 2 has the appearance of the vesicles snapping into contact, perhaps in response to some instability that developed previously. Video replay and quantitative analysis do, however, reveal measurable kinetics in this regime.

Phase 3 involves continued adhesion, manifested by slow growth in the contact angle and evolution of the projection lengths, especially that for the lower tension vesicle. Often the experiment ended during phase 3 when the low-tension vesicle escaped its pipet, as was the case in Figure 3. Upon escape from the pipet, the contact angle decreases back to a relaxed, if not equilibrium, value (from the mechanics perspective).

Figure 4 quantifies the adhesion and spreading processes for the vesicles imaged in Figure 3. In part A of Figure 4, the projection length evolution is shown for the left and right vesicles. It is the case for the vesicles in Figure 3 (and also generally true) that the projection on the high-tension side increased and that on the low-tension side decreased during spreading. This behavior was not generally seen in other laboratories (or in different studies in our laboratory) where the high-tension projection was static. Also, it is worth noting that during phase 1, prespreading, with nearly spherical vesicles, the LaPlace equation adequately describes the membrane tension. However, once the vesicles deviate substantially from spheres, it becomes necessary to calculate the membrane tension by measuring the total skin area of each vesicle and back-calculating τ from the mechanical property data of Figure 2. We found in these studies that despite the dramatic phase 2 changes in vesicle shape and projection length, the membrane area and volume were constant to within a few percent, the error in measuring nonspherical vesicle areas. This is consistent with the constant suction experimental protocol. Part B of Figure 4 focuses on features related to adhesion and spreading: the contact angle and the height or length of the contact region (defined in Figure 3). In phase 2, these evolve rapidly, and the abrupt onset of their growth, which defines the beginning of phase 2, is suggestive of an instability. It was generally observed that the growth in contact height was more abrupt and shorter lived than that of the contact angle, with the fastest evolution of the contact height in phase 2 typically finished within 1−3 s. The break between phases 2 and 3 was therefore a matter of judgment, identifiable by eye within a margin of a few seconds. For the vesicle pair in Figure 3, phase 2 lasted just under 10 s, which was typical of all the data: For the 18 vesicles studied, phase 2 lasted 20 s or less, and for 8 vesicles, it lasted 10 s or less, showing no dependence on the tension in either

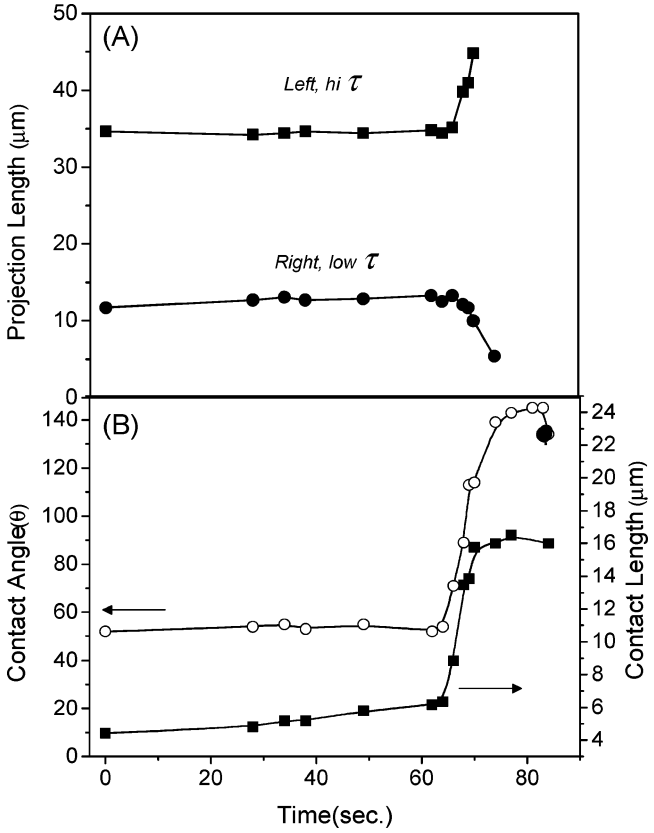

Figure 4. Quantitative adhesion dynamics with the vesicle pair from Figure 3: (A) left and right projection lengths and (B) contact angle and contact height, *h*, as a function of time. In (B), the contact angle relaxes downward after the vesicle escapes the right pipet, shown by the solid circle.

pipet. Also, during phase 2 for the vesicle in Figures 3 and 4, the contact angle and contact length growth rates were 13 deg/s and 2 μm/s, typical of other vesicles in this study (2−14 deg/s and 0.8−7 μm/s).

The particular run in Figures 3 and 4 terminated with the escape of the low-tension vesicle from its pipet during phase 3, which was common. It is worth noting, however, that in Figures 3 and 4 and in general that, at the time of vesicle escape, the contact angle was continuing to grow, not yet having reached its maximum value. Were the initial projection length of the low-tension side longer, escape from the pipet would have been delayed, so that a greater contact angle would have been achieved. Indeed, for vesicles with short initial projections, vesicle escape occurred in phase 2. These prematurely terminated runs were not counted among the 18 we report here. (The initial flaccidity or initial projection length is a random trait that depends not only on the osmolarity difference between the solutions inside and outside the vesicle but also on the intrinsic area/volume ratio of the vesicle during electroforming.)

In a few cases, vesicles with very long initial projections elucidated the terminal adhesion behavior. Here, phase 3 was protracted, and we observed a compromise of the vesicle membrane: either sudden rupture or evidence for leakiness, with the vesicle volume decreasing more rapidly than would occur due to slow evaporation from the chamber and slow water transport across the vesicle membrane. It may be that large numbers of avidin−biotin bonds formed in the junction between the two vesicles compromise the bilayer structure. We never did observe membrane fusion, however, or transfer of F-NeutrAvidin from one vesicle to the other. When vesicle rupture occurred, a small cap, consisting of the remains of the broken vesicle which resealed on itself, remained adhered to the partner vesicle, as shown in Figure 5.

Adhesion Strength. In this work, measuring the adhesion strength was a challenge because the contact zone was irreversibly bound in the practical sense: All attempts at peeling the vesicles apart, either by increasing tension or pulling back on the pipet, resulted in membrane rupture (or release of a vesicle from its pipet), with no reduction in contact area. Such peeling experiments were attempted by reaspirating the low-tension vesicle which had escaped its pipet during phase 3. Slow peeling forces (0.02−0.04 (mN/m)/s) were applied, which would tend to increase the chances for avidin−biotin bond disruption, relative to faster peeling. The contact time prior to peeling did not affect the results: Once adhesion began, the contact region could not be divided. Membrane rupture occurred between 1.5 and 4 mN/m, setting a lower bound on the adhesion strength.

Adhesion strength values in the range 1.5−4 mN /m are not particularly large. A point of comparison, the reversible depletion attraction (typically considered weak) induced by free polymer can be as large as 0.5 mN/m depending on the polymer molecular weight and concentration, in agreement with mean field calculations.[10] Our lysis values of 1.5−4.0 mN/m, which represent a lower limit for the adhesion of the avidin−biotin system, exceed depletion attractions by no more than an order of magnitude, arguing that the lysis energies are also weak, especially compared with the avidin−biotin adhesion. Therefore, the irreversible nature of the observed avidin−biotin membrane adhesion suggests that the actual adhesion strength in our case is much much greater than this observed lower limit of 4 mN/m.

It is worth noting that the literature on membrane adhesion driven by avidin−biotin binding is varied. Some laboratories employing two contacting phosophophlipid membranes find essentially permanent binding like us,[6] but other laboratories investigating biotinylated copolymer vesicle adhesion to avidin-coated beads report weak peeling tensions, with a maximum of 0.45 mN/m, depending on the biotin density.[11,23,25,36] Hence, for the scenario of modified copolymers, our adhesion measurements indicate greater binding forces than those of other laboratories.

Interpreting Constant-Tension Data in Terms of Spreading. The data measured at constant tension represent fascinating wetting behavior, where the time scales of the most dramatic and rapid features exceed those of membrane diffusion. Even in the limit of irreversible avidin−biotin binding exceeding the membrane strength, one might imagine various scenarios (densities of avidin−biotin cross-bridges, different tethering schemes) giving rise to different levels of strong adhesion (relative to the membrane cohesion). Such differences, not accessible via peeling, might be apparent in the wetting and spreading behavior. Hence, the work to pull two vesicles apart should not be the only means to gauge adhesion.

Following the theory of Bell et al.,[37] Noppl-Simson[6] identified the spreading pressure as being related to the chemical driving force for liposome adhesion and used it to quantify the density of avidin−biotin cross-bridges in the contact zone. The excess spreading pressure of avidin (bound to biotins across the adhesive plaque), $\Delta\Pi_{Av}$, which increases as spreading proceeds, is the summation of the surface pressures, Π_I, for the various avidin components within and outside the contact zone:

$$\Delta\Pi_{Av} = \Pi_{Av}(c_x^p) - \Pi_{Av}(c_u^p) + \Pi_{Av}(c_u^r) \qquad (2)$$

Here $\Pi_{Av}(c_x^p)$ is the spreading pressure of cross-bridged avidin in the adhesion plaque, while $\Pi_{Av}(c_u^p)$ and $\Pi_{Av}(c_u^r)$ are the

(37) Bell, G. I.; Dembo, M.; Bongrand, P. *Biophys. J.* **1984**, *45*, 1051−1064.

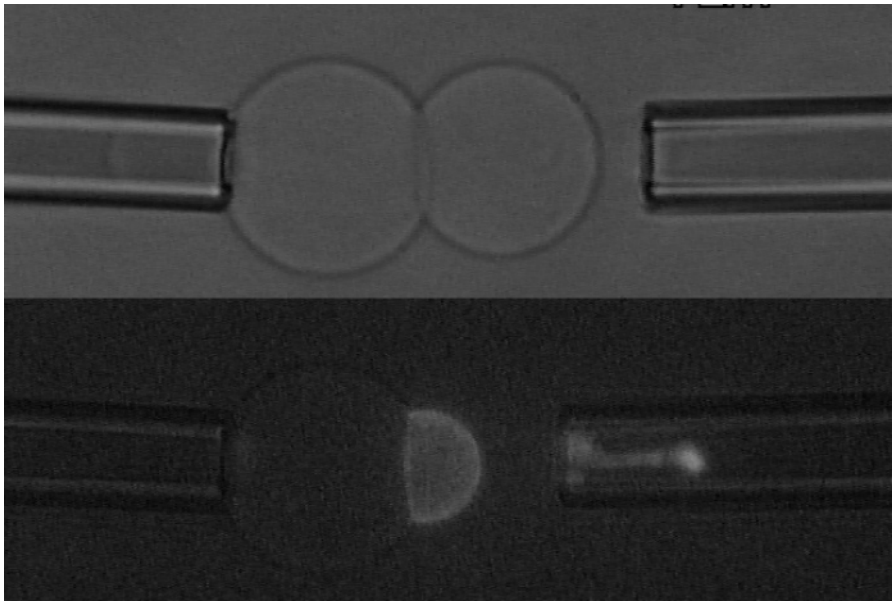

Figure 5. Top: Adhered vesicle pair after the right vesicle escapes the pipet. The right vesicle is subsequently reaspirated into the right pipet and suction increased until it breaks. The bottom image, with fluorescent illumination, shows that the adhesion plaque is not altered by this attempt at peeling, that no F-NeutrAvidin is transferred from the right to the left vesicle, and that part of the right vesicle reseals on itself after rupture.

spreading pressures of un-cross-bridged avidin in the plaque and in the rest of the vesicle, respectively. Each of these surface pressures, in the limit of 2-D ideal solution membrane behavior, is exclusively a function of the concentration of each species. In the Noppl-Simson study, the concentration of biotins and avidins on the membrane was 5 mol % or less: With the assumption that the strong binding of avidin and biotin caused all the avidin in the contact zone to be bound to biotin and with diffusion of avidins and biotins from the rest of the vesicle into the contact zone to strengthen the adhesive plaque, the situation in this dilute study was one where the receptor concentration in the contact zone eventually exceeded that in the rest of the vesicle, producing the excess spreading pressure. (Indeed, the movement of these receptors into the adhesive plaque was thought to be diffusion limited.) In the current work, this perspective on the spreading pressure breaks down for two reasons: The first is the densely functionalized nature of the vesicle surfaces. At the start our experiments, the portions of the vesicles that ultimately join to form the adhesion plaque already contain their maximum densities (or nearly so) of avidin and biotin. (Given this jammed interface and the need for molecular mating across the interface, it is quite likely that, in the plaque, not all the avidins and biotins are mated, but rather some remain unjoined as a result of kinetic jamming.) The second reason is that, with four binding sites per avidin, and an average of two biotins per copolymer chain, the avidinated vesicle is very likely cross-linked, preventing diffusion between the contact zone and the rest of the vesicle. Therefore, in our studies, were the spreading pressure approximated by concentration, per Noppl-Simson, it would vanish identically at all instances during an adhesion run.

Despite the breakdown of the spreading pressure argument, it remains useful to consider a chemical driving force for adhesion which, at equilibrium, is balanced by a mechanical opposing force: the membrane tension and geometrical factors. The relevant mechanical counterforce is $\tau_L(1 - \cos\theta)$, where τ_L corresponds to the lower of the two membrane tensions (because the lower tension vesicle does more of the spreading than the high-tension side) and θ is the evolving contact angle. In works where the vesicle adhesion is reversible, $\tau_L(1 - \cos\theta)$ has been equated with the reversible work of adhesion.[10] In the adhesion studies

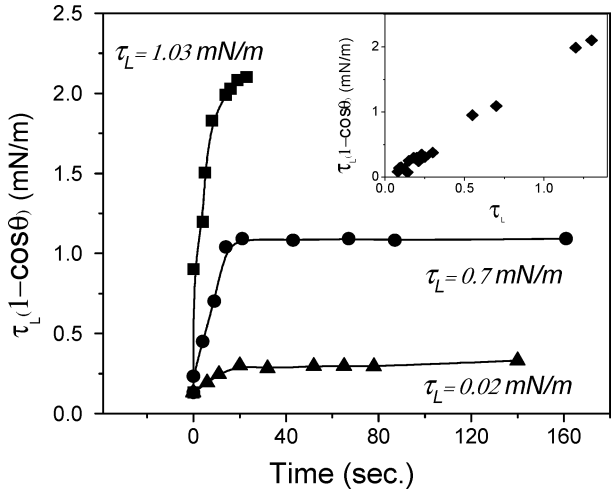

Figure 6. Representative plots of the evolution of the mechanical force as a function of time, for three different vesicles, at different tensions on the right side. The inset shows the ultimate values as a function of the tension in the right vesicle for all vesicles studied. The right membrane stress is designated τ_L because it is the lower of the two vesicles and the high stress on the left merely holds the left (substrate) vesicle in place.

of Noppl-Simson, this quantity was set equal to the spreading pressure, with the assumption of mechanical equilibrium at each instance of the relatively slow spreading study. In the current work, with the rapid spreading at the onset of phase 2, it would seem that the chemical driving force for spreading exceeds this mechanical counterforce.

Figure 6 shows the evolution of $\tau_L(1 - \cos\theta)$ with time for three representative vesicle pairs (all constant-tension) involving different suctions on the low-tension vesicle. Here, time zero corresponds to the beginning of phase 2, and in all cases, a rounding off in phase 3 is apparent before the lower tension side of each vesicle pair escapes its pipet. In general, experiments with greater values of the low vesicle tension were able to access greater values of $\tau_L(1 - \cos\theta)$. It is worth noting that, for a particular value of τ_L, $\tau_L(1 - \cos\theta)$ is bound with a maximum value of $2\tau_L$ when θ approaches perfect spreading of 180°. Thus,

the spreading curves, at constant tension, must ultimately plateau, though these runs ended in escape from the pipet.

Besides the general shapes of the curves in Figure 6, another important point is the magnitude of $\tau_L(1 - \cos\theta)$ accessed in these experiments: Values near 2 mN/m were consistently obtained with low-side membrane tensions exceeding 1 mN/m, far exceeding the maximum spreading pressures reported by Noppl-Simson for more sparsely functionalized liposomes (on the order of 0.1 mN/m = 0.1 dyn/cm), and also exceeding the critical peeling work of densely functionalized polymer vesicles reported by Lin et al. (0.45 mN/m)[11,23] which includes a dissipative component.

A second important point about Figure 6 is that the three curves, at different τ_L values, do not collapse. Instead, the ultimate values of $\tau_L(1 - \cos\theta)$ for each of the 18 runs are proportional to τ_L, as shown in the inset of Figure 6. That is, the ranges of time scales and ultimate contact angle values accessed in all the runs are very nearly similar, though $\tau_L(1 - \cos\theta)$ should be more relevant to adhesion than the contact angle alone. This is a quantitative indication that the chemical driving force for adhesion in our experiments far outweighs any opposing mechanical forces, consistent with the rapid phase 2 spreading observed. The three data sets in Figure 6 employed vesicles with the same receptor density and presumably the same chemical driving force for adhesion. Were this chemical driving force balanced by the mechanical counterforce, $\tau_L(1 - \cos\theta)$, then this counterforce would be identical for all three experiments, and for higher values of the imposed τ_L, θ would compensate so that the curves would collapse. Indeed, Noppl-Simson et al. never explicitly report their τ_L values, but rather present only spreading pressure or $\tau_L(1 - \cos\theta)$ data, implying that their data did indeed collapse (i.e., that the exact value of τ_L was unimportant). Because the mechanical force in the current constant-tension studies has little influence on how spreading proceeds, it is implied that the chemical adhesive strength is much larger than the O(1 mN/m) mechanical counterforce, which represents a lower bound to the adhesive strength of our system.

Ramping the Low-Tension Membrane. Since the constant-tension studies imply the chemical driving force for adhesion far exceeds the mechanical counterforce against spreading, always giving rapid phase 2 spreading independent of fixed τ_L, we were motivated to consider a second experimental protocol: We made the high-tension vesicle as tight as possible and began with the low-tension vesicle at small or moderate suction before putting the two vesicles in contact. Then, once phase 2 spreading was under way, we increased the low-tension suction in an attempt to provide a force which would at least temporarily arrest the spreading process.

This approach was of interest for two reasons: First, for practicality, it allowed us to access higher membrane tensions than the constant-tension protocol. In the constant-tension approach, when relatively high tensions were applied to the two vesicles prior to contact, many vesicles broke before adhesion began. In the ramp protocol, if the low-tension vesicle broke as we ramped its suction, the experiment would terminate, but we would still have data on the initial spreading kinetics. Scientifically important, the ramp protocol focuses on adhesion at short times, with limited numbers of avidin−biotin contacts (before additional bonds can form through interfacial reconfigurations). One might imagine that on time scales of seconds or shorter, the driving force for adhesion would involve the avidins and biotins that were oriented for immediate engagement. At the longer time scales a greater adhesive driving force might result from the rotational diffusion of avidins and biotins on the PEG chain ends, or the diffusion of buried biotins and avidins from beneath the outer surface of the corona (or the diffusion of longer PEG strands out of the way of avidin−biotin approach).

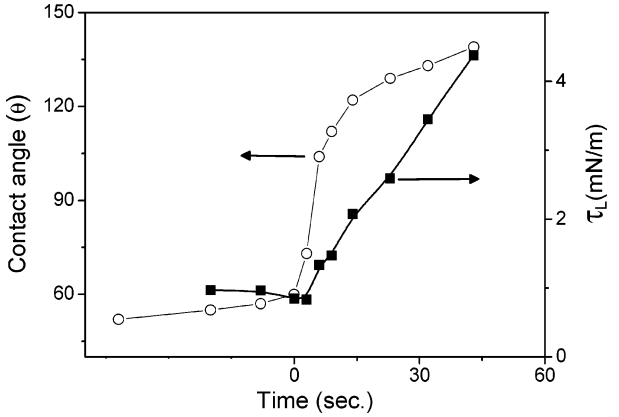

Figure 7. Example of vesicle adhesion when the right (lower) vesicle tension is ramped up during phase 2 of spreading.

Figure 7 shows a particularly interesting example of a ramp experiment: Initially, two vesicles were put into contact with the low-tension vesicle near $\tau_L = 0.9$ mN/m. At the onset of phase 2, we increased the low-tension side (on the right axis) and found that we were unable to stop the growing vesicle contact and contact angle. While in this particular example the rate of increase in τ_L is modest extending into phase 3, the contact angle continued to grow until the vesicle was pulled out of the pipet. We were unable to hold onto the vesicle, even with a tension of 4 mN/m. We have another example of ramp procedures in which the increase in τ_L was sharper (up to 0.2 (mN/m)/s); however, we were never able to arrest spreading or prevent vesicles from escaping the pipet (though we did break the vesicles in a number of cases). Of note for the particular run in Figure 7, the value of $\tau_L(1 - \cos\theta)$ exceeds 7 mN/m before the vesicle escapes the pipet. This is the largest mechanical resisting force we were able to measure, indicating an even larger driving force for adhesion than was measured at constant tension.

From this we conclude that the spreading process, driven by the formation of avidin−biotin bonds at the contact line, has a much greater forward rate constant than any elastic or mechanical resistance by the membrane. This does not seem so remarkable at first given the dense membrane functionalization in the current work; however, of the avidins and biotins at the moving contact line, one expects only a fraction to be available for immediate bonding as others may be oriented incorrectly or buried within the bilayer brush, as is suggested by the effect of functionalization on the membrane mechanics in Figure 2.

Summary

The adhesion of NeutrAvidin- and biotin-functionalized membranes, in the limit of dense receptor functionality, follows kinetics best described in three phases. Early adhesion involves minimal deformation of the vesicle membrane; however, at some point marking the start of phase 2, the vesicles snap into contact abruptly in a manner that deforms both vesicles. Beyond this time, in phase 3, the contact angle continues to grow as the adhesion strength evolves. Runs terminate with the escape of vesicles from the micropipet or the compromise of the membranes themselves. The rapid snapping into contact, not mentioned previously in the vesicle adhesion literature, is reminiscent of an instability, for instance, that seen during the approach of an AFM tip to a surface or in the surface forces apparatus. During the onset of rapid adhesion, the adhesion rates were as high as 7

μm/s, or 14 deg/s, greater than other values we find in the literature and likely a direct result of the irrelevance of lateral receptor diffusion to the adhesion mechanism. Indeed, for the time scales involved (no more than a few seconds and often much less), the adhesion plaque growth is likely controlled by the rate of membrane bending and the energy dissipation involved in progressive bending.

Consistent with expectations for strong NeutrAvidin−biotin interactions, NeutrAvidin−biotin-driven membrane adhesion is irreversible, preventing peeling apart of the adhesion plaque at experimentally accessible rates. Membrane cohesion strengths as large as 4 mN/m (4 mJ/m^2) set the lower bound on the membrane adhesion strength. This value, when used to calculate the minimal mechanical force of adhesion, $\tau_L(1 - \cos\theta)$ exceeds, by over an order of magnitude, that reported previously for biotinylated liposomes in the more dilute membrane functionalization limit, though those latter results also were sufficiently strong to prevent peeling. The adhesion values reported here also exceed those reported for biotinylated copolymer vesicle interactions with avidin-coated beads, over the full range of receptor surface densities.

For runs at fixed surface receptor density, but in which the low tension, τ_L, is varied by over an order of magnitude, the spreading rate curves fail to collapse when $\tau_L(1 - \cos\theta)$ is plotted as a function of time, unlike the implications from other laboratories. This suggests that the mechanical resisting force is much smaller than the chemical driving force for adhesion. Hence, the system in this work may be one of the strongest membrane adhesive systems reported thus far.

Acknowledgment. This work was supported by NSF Grants CTS-0428455 and CTS-0242647 and NSF MRSEC Grant DMR-0213695. We thank R. Hill of Dow Corning for helpful discussions and pointing us in the direction of DC5329.

LA700542T